Materials Today Physics 48 (2024) 101562

Contents lists available at ScienceDirect

Materials Today Physics

journal homepage: www.journals.elsevier.com/materials-today-physics

A high stretchability micro-crack tactile sensor system based on strain-isolation substrate

Xiaojun Pan [a,b], Jing Li [b,d], Zhangsheng Xu [b,d], Yue Liu [b,d], Wenchao Gao [b,***], Rongrong Bao [a,b,c,d,**], Caofeng Pan [a,b,c,d,*]

[a] Center on Nanoenergy Research, Key Laboratory of Blue Energy and Systems Integration, School of Physical Science & Technology, Guangxi University, Nanning, Guangxi, 530004, PR China
[b] Beijing Institute of Nanoenergy and Nanosystems, Chinese Academy of Sciences, Beijing, 101400, PR China
[c] Institute of Atomic Manufacturing, Beihang University, Beijing, 100191, PR China
[d] School of Nanoscience and Engineering, University of Chinese Academy of Sciences, PR China

ARTICLE INFO

Keywords:
Strain-isolation substrate
High stretchability sensor system
Micro-crack sensor

ABSTRACT

The integration of inflexible constituents onto pliable substrates is widely acknowledged as the most pragmatic approach for the realization of stretchable electronics. Nevertheless, the assurance of enduring connectivity between rigid electrode components and these compliant substrates poses a formidable quandary. In the scope of our investigation, we proffer a resolution by conceptualizing a PDMS substrate replete with strain isolation partitions, which can generate Young's modulus difference of approximately 30 times. These partitions efficaciously safeguard the steadfast linkage between rigid components and electrodes, even under diverse strain provocations, a stable connection can be maintained even when able to withstand strain exceeding 120 %. Using this substrate, we constructed a visual deformation sensing system based on microcrack type sensors. Compared with traditional flexible substrates (2 % strain), systems based on strain isolation substrates have better tensile stability (10 % strain). This groundbreaking innovation bestows stretchable micro-crack strain-sensing systems the resilience to contend with the potentially formidable rigors of everyday application.

1. Introduction

Stretchable electronics denote electronic apparatus engineered to sustain their conventional functionality even under conditions of extension, flexure, or deformation. These pioneering contrivances possess the capacity to conform to cutaneous surfaces, accommodating the anatomical nuances and dynamic movements of the human physique. This attribute engenders more precious data acquisition while concurrently enhancing the comfort and steadfastness of wear. The emergence of stretchable electronics is heralded as a transformative development in the realm of electronics, promising to chart new frontiers by enabling access to hitherto inaccessible domains [1–5].

Within this context, strain sensors are designed to exhibit mechanical response to applied strain, thus resulting in discernible alterations in their electrical properties, chiefly in terms of resistance or capacitance [6,7]. In contrast to their counterparts within the spectrum of stretchable electronic devices, strain sensors confer a multitude of advantages including but not limited to their pronounced sensitivity [8–10], high response speed [11–13], and cost-effective production methodologies. As a consequence, they have been applied in various fields [14], including motion detection [15–17], health surveillance [18–20], human-computer interaction [21–23], and human work capture for entertainment systems [24]. Practical exigencies within these fields continually underscore the necessity for augmented sensitivity in stretchable electronic devices to ensure precision in measuring minute strains.

To ensure the effective integration of micro-crack sensors into diverse application scenarios, it is imperative to establish a

* Corresponding author. Center on Nanoenergy Research, Key Laboratory of Blue Energy and Systems Integration, School of Physical Science & Technology, Guangxi University, Nanning, Guangxi, 530004, PR China.
** Corresponding author. Center on Nanoenergy Research, Key Laboratory of Blue Energy and Systems Integration, School of Physical Science & Technology, Guangxi University, Nanning, Guangxi, 530004, PR China.
*** Corresponding author.
E-mail addresses: gaowenchao@binn.cas.cn (W. Gao), baorongrong@ucas.acs.cn (R. Bao), pancaofeng@buaa.edu.cn (C. Pan).

https://doi.org/10.1016/j.mtphys.2024.101562
Received 22 June 2024; Received in revised form 14 September 2024; Accepted 26 September 2024
Available online 27 September 2024

comprehensive crack-type strain sensing system, consisting of both the sensor component itself and a signal processing unit. Nevertheless, two pivotal aspects require urgent attention within the construction of strain-sensing systems. First and foremost, a common issue arises from the use of different materials between the sensor's sensitive layer and the electrodes, frequently giving rise to challenges concerning the preservation of a stable connection throughout the strain-induced deformation process [25,26]. Secondly, a pronounced disparity in Young's modulus exists between the non-extensible rigid elements inherent in the signal processing unit and the elastic substrate [27]. This incongruity presents formidable obstacles in the seamless adaptation of the rigid signal processing unit to the inherently elastic nature of the strain system. The resolution of these issues stands as a fundamental imperative in augmenting the functionality and dependability of crack-type strain sensors across a diverse array of application domains.

A comprehensive strategy has been formulated to concurrently ameliorate the aforementioned issues through the introduction of Young's modulus patterned partitioning on an elastic substrate. This strategy effectively resolves dilemmas pertaining to the connection between the sensitive layer and the electrodes and the stable operation of rigid components under the influence of mechanical strain. This is achieved through the judicious incorporation of varying Young's modulus distributions across the substrate. In this strategy, zones with a lower Young's modulus experience heightened strains during deformation, while regions with a higher Young's modulus are insensitive to these mechanical strains [28,29]. Currently, strain isolation strategies are predominantly implemented using the following methodologies. Firstly, Material Selection with Young's Modulus Differences: The strategy involves the deliberate selection of materials with significant differences in Young's modulus, exemplified by the embedding of rigid components directly within an elastic substrate [30]. Secondly, Multilayer Material or Component: Design materials or components featuring multilayer structures, each endowed with distinct Young's modulus values, which serves to evenly distribute stresses and enhance material strength [31,32]. Thirdly, Geometric Alterations: The strategy entails the introduction of apertures, protrusions, or other geometric configurations into specific substrates via alterations in material composition or geometric structure [33,34]. Nonetheless, persisting issues with these strategies are urgent to be solved. Firstly, the achievement of patterned Young's modulus partitioning within a substrate often demands complex design and fabrication processes, such as photolithography, which may result in elevated costs. Secondly, it is imperative to formulate solutions conducive to facile large-scale preparation suitable for commercial applications. Lastly, the introduction of diverse material constituents can engender issues pertaining to material compatibility and interface discrepancies, thus mandating supplementary solutions during practical utilization. The effective resolution of these challenges is pivotal in propelling the development of Young's modulus patterned partitioning for strain sensors across diverse application domains [35,36]. Here, a strategy has been proposed to address the previously mentioned challenges and enable the convenient and stable preparation of large-scale substrate Young's modulus patterning by introducing Young's modulus changes through secondary curing of Polydimethylsiloxane (PDMS).

In this research, we have undertaken the fabrication of PDMS substrates with differences in Young's modulus through a two-step method, thereby achieving a substantial contrast in Young's modulus (approximately ~30) on a single PDMS substrate. The modulation of PDMS Young's modulus has resulted in the induction of varying crack densities within the same PDMS substrate, which generates disparate mechanical responses to strain within distinct regions of the substrate. Finite element simulation analysis shows that the strain isolation substrate can generate an 8-fold strain difference between the two regions when applied with 2 % strain. This demonstrates the efficacy of the strain-isolated substrate in effectively shielding regions with higher Young's modulus from experiencing strain-induced deformation during external mechanical perturbations. Consequently, this mechanism ensures the durability and functionality of the device, especially in regions with higher Young's modulus. To verify the durability of the interconnection between the strain-isolated substrate and the standard substrate, as well as the electrode elements, experimental comparisons were conducted. The electrodes can apply 120 % strain on the strain-isolated substrate and still have a stable connection to the substrate. Compared to the light-emitting diodes (LEDs) installed on traditional flexible substrates, the circuits located on strain-isolated substrates exhibit higher tolerance to complex external conditions (increased by 5 times). This was predominantly realized through the establishment of a stable connection between the rigid electronic components and the external interfaces during the strain-induced deformation process, effectively preserving the structural integrity of the rigid components, particularly when subjected to tensile forces. It is imperative to emphasize that this study is primarily centered on the assessment of strain isolation strategies intended to safeguard rigid components from mechanical strain, which furnishes valuable insights into the design of stretchable electronic systems.

2. Results and discussion

Fig. 1a illustrates the structural configuration of the crack strain sensing system, consisting of rigid components and electrodes in the high Young's modulus region to establish a robust connection. Simultaneously, the system incorporates an elastic substrate with low Young's modulus to ensure the overall device's stretchability. The inset in Fig. 1a provides a visual exposition of crack formation occurring during tensile deformation in both the high Young's modulus and low Young's modulus regions. Notably, a substantial disparity in crack density is evident, with the high Young's modulus region displaying significantly lower crack density in comparison to the low Young's modulus region. The stress-strain curve depicted in the right-side illustration emphasizes the substantial difference in Young's modulus between these two regions, serving as a crucial prerequisite for our subsequent applications. In the preparation of the PDMS substrate, our initial step involved the meticulous blending of PDMS oligomer and curing agent in a 20:1 ratio, culminating in the formation of a PDMS substrate with low Young's modulus. The vinyl groups located at both terminals of the oligomer partake in a chemical reaction with the *Si*-H bonds present in the curing agent, giving rise to the establishment of an intricate three-dimensional network structure. Subsequently, the curing agent is uniformly deposited onto the pre-prepared PDMS substrate through spin-coating at various rotational speeds. This procedure enables the curing agent to continue its reaction with unreacted vinyl moieties within the PDMS film, leading to the formation of a more intricate three-dimensional network and, consequently, a modification in the material's Young's modulus, as depicted in Fig. 1b. A detailed account of the fabrication process for the proposed strain sensor employing a strain-isolated substrate is delineated in Fig. S1, Supporting Information. For a comprehensive understanding of the experimental procedures and outcomes, readers are directed to consult the corresponding section.

To assess the variation of PDMS mechanical properties during the secondary cross-linking curing stage, PDMS films produced via spin-coating the curing agent at varying rotational speeds were subjected to mechanical testing utilizing a dynamometer, as visually represented in Fig. S2a, Supporting Information. The PDMS membranes resulting from each treatment condition were subsequently fashioned into rectangular cubes, measuring 4.0 cm in length, 1.0 cm in width, and 0.1 cm in thickness. The stress-strain curves obtained from the polymer PDMS films reveal a discernible trend: as the rotational speed of the spin-coated curing agent increases, the stress-strain curve progressively converges towards the behavior observed in untreated PDMS films that did not undergo secondary curing treatment. The slope of these stress-strain curves was employed to ascertain Young's modulus of PDMS at varying rotational speeds for the spin-coated curing agent, as exhibited in Fig. S2b, Supporting Information. The results demonstrate a gradual

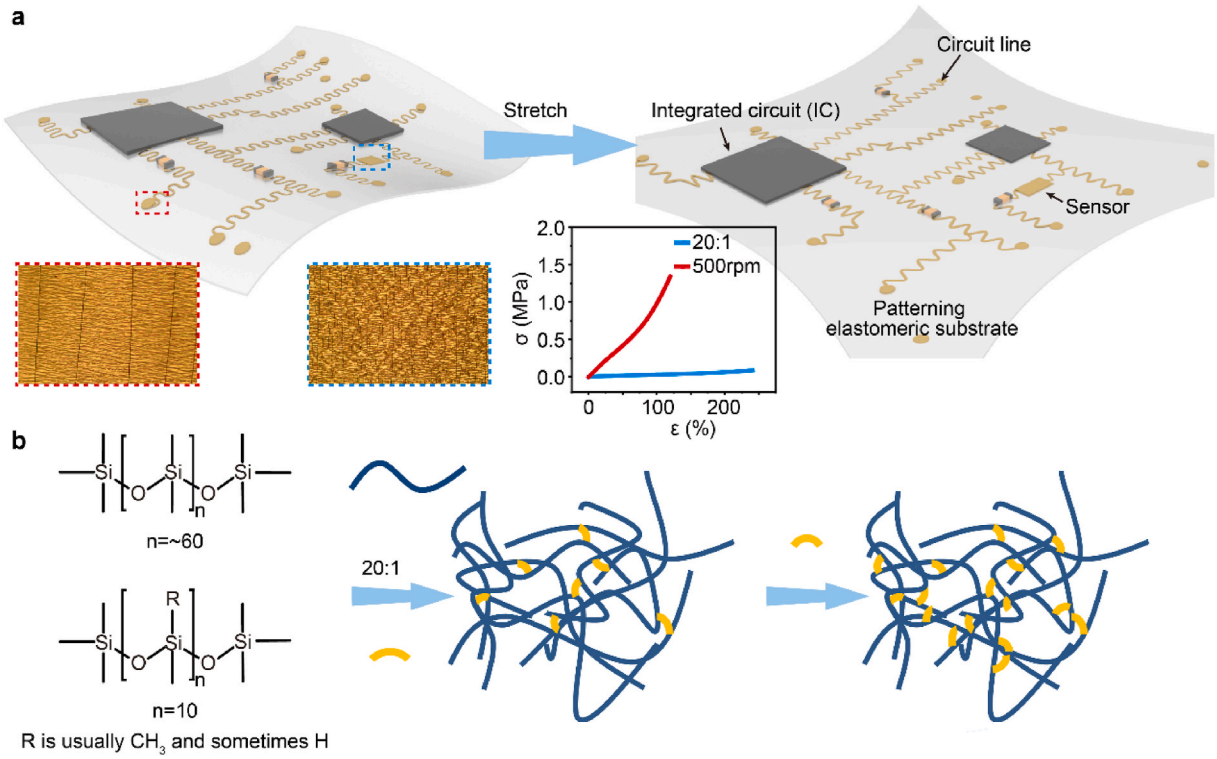

Fig. 1. Strain isolation strategy. a) Schematic diagram of a stretchable circuit based on a strain-isolated substrate. The inset shows optical microscope photos of the crack morphology in different regions and the stress-strain curves of the two parts. b) Chemical formula and cross-linking process of each component of PDMS.

reduction in Young's modulus with the rotational speed of the spin-coated PDMS curing agent increasing, covering a range from 0.026 MPa to 0.82 MPa. This variation underscores the diminishment in tensile properties attributable to the presence of the curing agents. In pursuit of optimizing strain isolation, untreated PDMS films featuring a substantial stiffness contrast (~32) and spin-coating at 500 rpm during the secondary curing process were deemed most suitable for serving as the sensitive layer and electrodes. This determination was predicated on the analysis of the stress-strain curve. Furthermore, as evidenced in Fig. S2b, Supporting Information, it is noteworthy that Young's modulus appears to converge around 500 rpm and 1000 rpm during the secondary curing process. This convergence can be attributed to the saturation of the chemical reaction between the curing agent and the pre-fabricated PDMS substrate.

The currently accepted interpretation for cracked stretchable strain sensors involves the disconnection and reconnection of cracked edges. When an elastic substrate with a positive Poisson's ratio is stretched in the axial direction, it compresses in the transverse direction. This behavior allows axial tension to disconnect the crack edges, while lateral compression can reconnect them [37]. In a quest to explore the implications of these cracks on strain-isolated substrates, we scrutinized the number of cracks present in PDMS films across diverse pre-stretching conditions and varied Young's modulus values. Notably, it was discerned that PDMS films endowed with Young's modulus of 0.026 MPa displayed a greater propensity for the development of heterogeneous cracks during the pre-stretching process when contrasted with films featuring divergent Young's modulus values (Fig. S3a, Supporting Information). In furtherance of our investigation, mathematical statistical analyses were employed to ascertain the crack density resulting from the pre-stretching of PDMS films characterized by differing Young's modulus values (Fig. S3b, Supporting Information). Higher Young's modulus films result in less cracks at the same tensile strain. Meanwhile, we count the cracks on the soft substrate (Fig. S3c, Supporting Information), and the crack density stays in a small range under the same pre-stretching conditions, indicating that although our method is able to maintain a good consistency overall. Compared to elastic substrates, the strain-isolated substrates have a lower crack density and still maintain good strain isolation for different substrate thicknesses. Furthermore, as the continued application of strain, the PDMS film developed new cracks with wider widths (refer to Fig. S4, Supporting Information). Regions distinguished by lower Young's modulus displayed a heightened prevalence of such cracks following strain stretching. By synergizing the strain isolation strategy with the elucidated mechanism underpinning the micro-crack sensor, we effectively demonstrate that it is feasible to substantially curtail the crack density within PDMS substrates. This, in turn, serves the dual purpose of shielding specific regions from strain-induced deformations while concurrently minimizing the impact of external mechanical stresses.

To demonstrate the efficiency of strain isolation, we fabricated PDMS films with distinct mechanical properties. One PDMS film was treated with a secondary spin-coating curing agent, resulting in a higher modulus of 0.82 MPa, while another PDMS film remained untreated, retaining a lower modulus of 0.026 MPa. Pentagrams were meticulously imprinted onto discrete regions of the PDMS film, as shown in Fig. 2a. After tensile deformation, the pentagram pattern persisted unaltered in the region with the secondary spin-coated curing agent. In contrast, an obvious distortion of the pentagram pattern was observed on the untreated PDMS film. This observation substantiates the viability of the PDMS partition curing approach. To expound upon this phenomenon, we conducted finite element analyses, as displayed in Fig. 2b and c. The computational model contained a strain-isolation substrate and an untreated substrate, both subjected to a 2 % strain with the length of 15 mm. The finite element analysis demonstrated the selectivity in stress-strain distribution exhibited by the strain-isolation substrate, in comparison to the uniform stress distribution of the untreated PDMS film. Under tensile, the strain localized in the untreated portion of the PDMS, while the stress concentration primarily occurred at the interface between the two regions, which is consistent with the experimental results in Fig. 2a. Fig. 2d further elucidates the strain distribution along the central axis at the top surface. Here, it is evident that the strain within

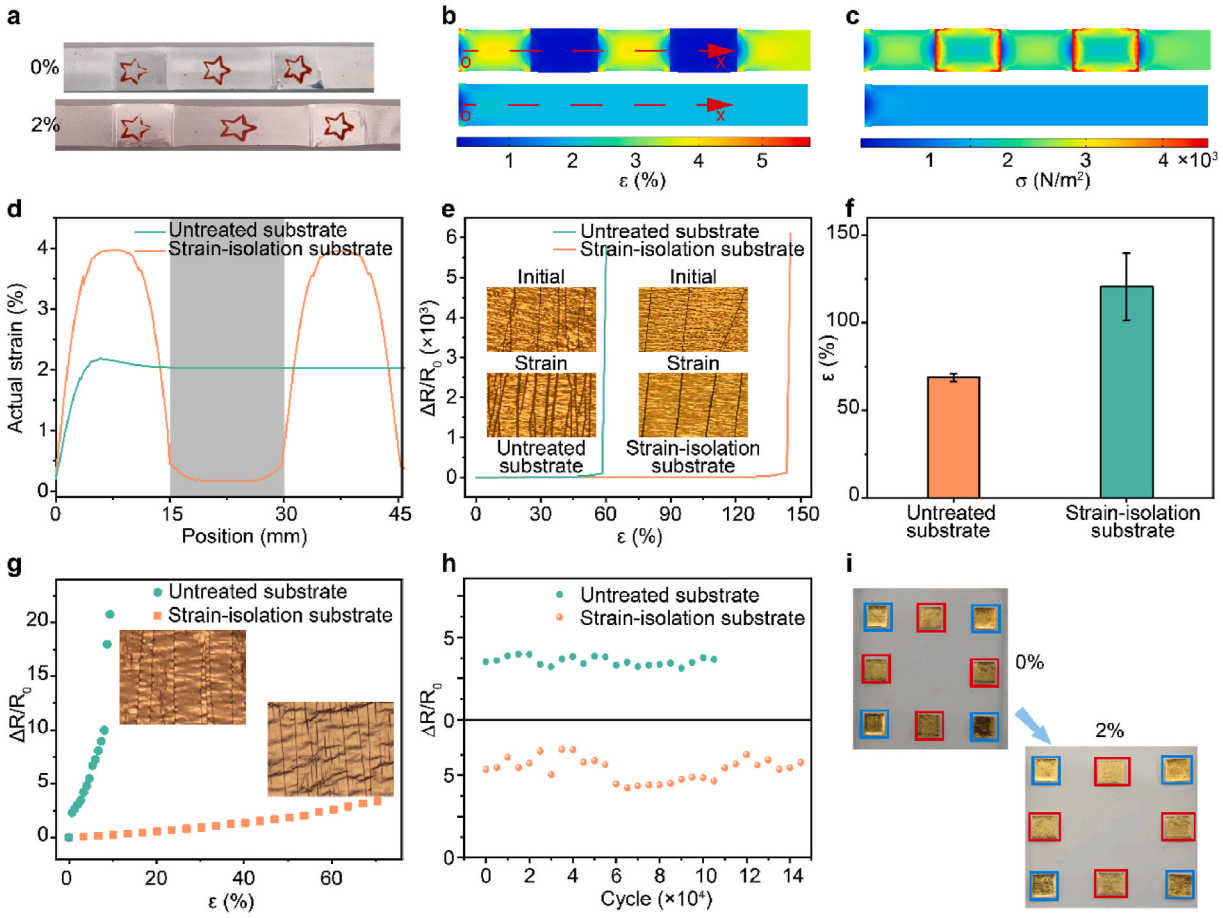

Fig. 2. Electrical and mechanical properties of strain isolation substrate. a) Visual illustration of strain isolation. b) Strain distribution at the top surface of the strain-isolated substrate under strain. c) Stress distribution at the top surface of the strain-isolated substrate under strain. d) Actual strain distribution (zero position corresponds to the origin of the x-axis in b). e) The strain on the wire separated from the substrate in different parts. f) Error statistics of the strain on the separation of the wire from the substrate. g) Untreated PDMS substrate and strain-isolated substrate as a function of tensile strain for micro-crack sensors, the inset is a picture of the crack under the optical microscope. h) Stability of strain-isolated substrate sensors versus common substrate sensors (under 2 %). i) Comparison of the gold film: the red rectangle is unprotected, blue rectangle is protected.

the untreated PDMS reached a magnitude of 3.96 %, while, it was notably reduced to a mere 0.17 % in the strain-isolated PDMS. In contrast, the strain distribution in the untreated PDMS film exhibited a relatively even distribution around 2 %. These results identified the efficiency of strain isolation achieved by localized treatment of the PDMS substrate, thus rendering it conducive for the placement of functional components.

Although the strain generated during sensor testing and utilization does not inherently induce damage to the performance of sensor, it is important to note that the electrode employed in testing may separate from the sensor due to the elevated levels of strain incurred during loading and unloading processes. Such separation can lead to sensor damage prior to its installation and operation. To demonstrate the effectiveness of the zoning strategy in mitigating damage occurring during the transport and installation, electrodes were deposited on PDMS films with and without strain isolation, respectively, and their stability during the stretching process was examined. All test devices were assessed with the copper wire directly connected from the electrode to the testing instrument, which frequently resulted in the disconnection of the copper wire from the electrode. As depicted in Fig. 2e, the electrode situated on the PDMS film with strain isolation exhibited a higher strain tolerance in comparison to the untreated PDMS film. Notably, the electrode of the strain-isolation PDMS film displayed fewer cracks and experienced fewer crack formations during the stretching process, as visually represented in the inset of Fig. 2e. Based on the experimental outcomes, it was determined that the wire became disconnected from the sensor on the untreated PDMS film at a strain of about 60 %, while the wire was connected with the sensor on the strain-isolation PDMS film until a strain of about 140 %. Fig. 2f exhibits several failure experimental results, which demonstrate that the strain-isolation substrates represent a higher tolerance of strain (~120 %) than the untreated substrate (~60 %).

PDMS films with different Young's modulus were employed as substrates for the preparation of strain sensors intended for strain-stretching assessments. As illustrated in Fig. 2g, it is evident that with the increase of strain, the electrical resistance of the untreated PDMS film experiences a sharp and pronounced increase, whereas the resistance of the strain-isolation PDMS film undergoes a more moderate increase, remaining below five times the initial resistance within the 60 % strain. This phenomenon can be attributed to the less crack formation in the strain-isolation PDMS film, a consequence of its elevated Young's modulus. In addition, the stability of the strain-isolated substrate was explored as shown in Fig. 2h and Fig. S5. The tensile testing included the electrode region. It was observed that the resistance of the conventional sensor commenced its ascent after approximately 19,000 cycles (under 2 % strain), while the resistance of the strain-isolated sensor remained stable for approximately 20,000 cycles. Compared to the untreated substrate, the strain-isolated strain sensor demonstrates superior performance stability, demonstrating the advantages of the strain-isolated substrate in terms of enhancing sensor stability. Fig. 2i provides a

more immediate and visual insight into the influence of strain isolation. A series of gold squares was magnetron sputter deposited onto the substrate, with some strategically positioned in the flexible region (marked in red, unprotected part) and others in the rigid region (marked in blue, protected part). After unidirectional stretching, conspicuous deformation was evident in the unprotected gold squares, standing in stark contrast to the pristine condition observed in the protected blue region.

The partitioning of Young's modulus on a PDMS substrate serves as an effective strategy for the challenge of unstable connections between rigid components on elastic substrates. Implementing a strain sensing system also requires the preparation of highly sensitive strain sensors. Fig. 3a illustrates the operational principle of the crack strain sensor. During the initial pre-tensioning process, some parallel cracks perpendicular to the pre-strain direction are generated, and after the release of the pre-strain, the majority of these cracks remain sealed, with their edges overlapping. This sealing phenomenon is pivotal for the sensor's efficacy. With the increase of the strain, the number of cracks gradually increases, and the mechanism governing changes in electrical resistance evolves from the overlapping effect to the tunneling effect, leading to a rapid surge in resistance under high levels of strain, as delineated in Fig. S4. The width and density of the cracks engendered during pre-stretching serve as determinants of the sensor's sensitivity. Greater crack density enables the sensor to exhibit heightened responsiveness to strain variations. The design objective of a crack strain sensor is to generate an increased density of cracks within the strain-sensitive region to facilitate heightened sensitivity to strain fluctuations, while simultaneously maintaining fewer cracks in the electrode connection area to mitigate the impact of strain changes on the electrode signal. Consequently, the control of crack density allows for the achievement of varying levels of sensitivity in the sensor. Cracks emerge as a consequence of the Young's modulus disparity between the elastic substrate and the metallic layer. Therefore, by adjusting the discrepancy in Young's modulus between the elastic substrate and the metallic layer, it is feasible to regulate the sensitivity of the strain sensor. In the regions with high Young's modulus, fewer cracks are generated during pre-stressing, rendering them suitable for stable electrode connections owing to their reduced sensitivity to strain. Conversely, regions with lower Young's modulus generate a greater density of cracks, which translates to heightened responsiveness to changes in strain, as shown in Fig. S3.

On this foundation, we engineered a crack strain sensor capable of maintaining a secure and robust connection with the protective electrode. The strength of a substrate is directly proportional to its Young's modulus and is inherently linked to the cube of the substrate's thickness [38]. Consequently, the thickness of the substrate plays a pivotal role in the formulation of strain sensors [39,40]. To further investigate the sensitivity of the crack strain sensor, we explored the impact of PDMS film with various thicknesses on sensor responsiveness. As shown in Fig. 3b, the relative change in resistance ($\Delta R/R_0$) in PDMS films of

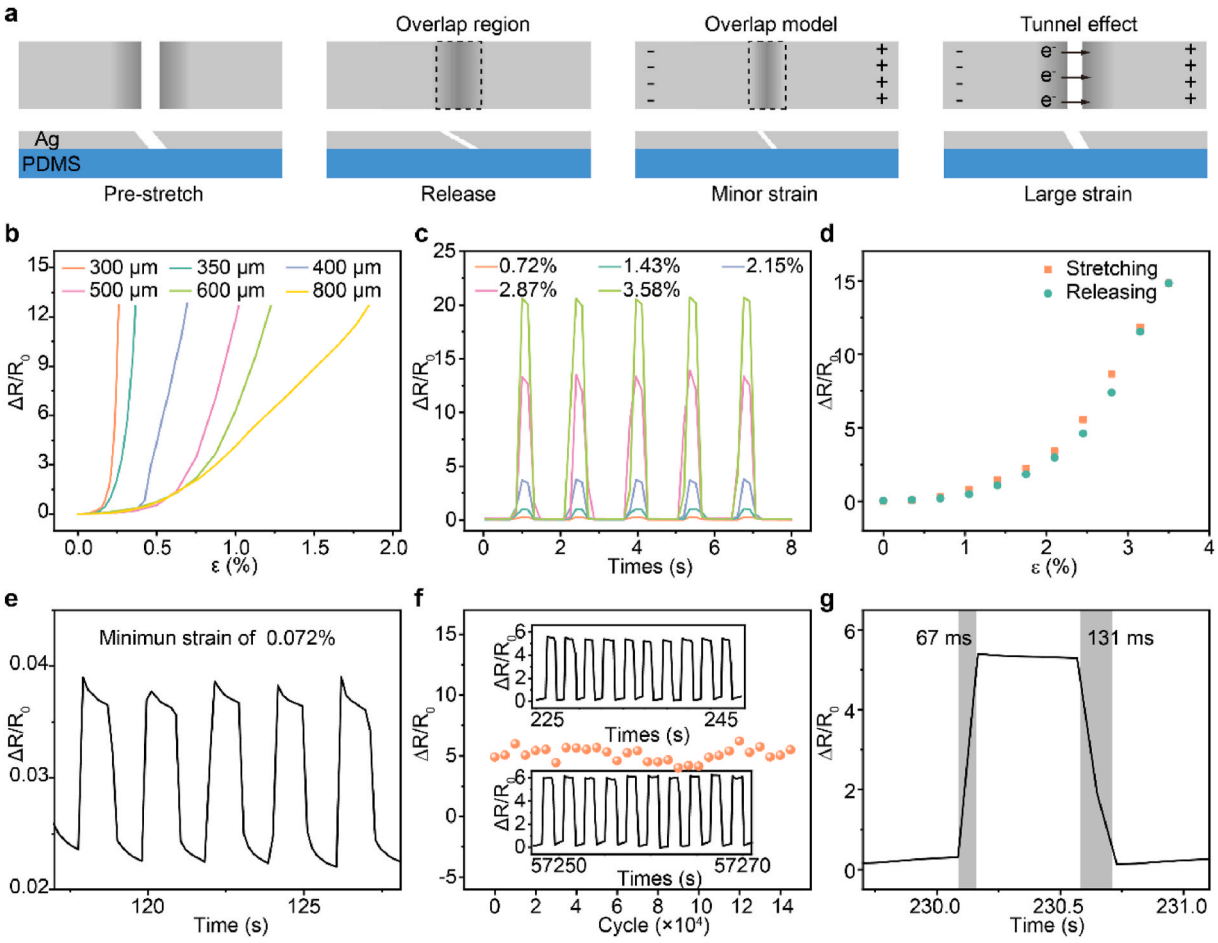

Fig. 3. Electrical properties of strain sensor. a) The proposed working mechanism of the micro-cracked strain sensor. b) Relative resistance variation of strain sensors based on strain-isolated substrates of different thicknesses. c) Five cycles of strain sensors based on strain-isolated substrates at different strains. d) R/R_0 variation under an individual stretching cycle with the strain of ~3.5 %. e) The minimum detectable strain limit of the sensor. f) The mechanical stability of the strain-isolated substrate sensor at 2 % strain. The inset is the period of the sensor response. g) The response time of the strain isolation sensor. Response time and recovery time are 67 ms and 131 ms respectively.

different thicknesses exhibited a pronounced increase with the imposition of strain. Notably, as the thickness of the PDMS films increased, the relative resistance changes gradually diminished in response to strain. This observation underscores the utility of thickness modulation in PDMS films as a viable strategy for tailoring the performance of strain sensors. Thinner PDMS films exhibit exceptional sensitivity yet exhibit poorer stability, whereas thicker PDMS films offer enhanced reliability at the expense of reduced sensitivity. Consequently, we selected a PDMS film thickness of 500 μm for the strain sensor, striking a balance that yields an optimal compromise between sensitivity (over 23000 at 2 % strain, Fig. S6) and overall performance, thus suitable for further electrical testing.

In the fabrication of the sensitive layer through magnetron sputtering, the thickness of the silver film exerts a significant influence on the initial resistance and the extent of relative signal response variation exhibited by the sensor. We conducted exploratory investigations with different sputtering times in Fig. S7, and observed a direct correlation between the sputtering time and the silver film thickness. As the sputtering time increased, the silver film thickened, leading to a concomitant reduction in the initial resistance and a decrease in sensitivity. Notably, the strain sensor exhibited remarkable stability and reproducibility across five consecutive cycles, each involving different strain levels (with a 0.7 % strain change), as shown in Fig. 3c. Also, our strain sensors maintain a good response to 3 % strain applied at different rates (Fig. S8). Fig. 3d displays the instantaneous response of the strain isolation sensor during successive tensile and release cycles with strains ranging from 0 % to 3.5 %, which demonstrates the sensor's flexibility and minimal hysteresis. However, it is worth noting that the relative resistance change from maximum strain release is slightly smaller than that observed during stretching at the same strain level. This diminishment can be attributed to the gradual recovery of PDMS following extensive stretching, which gives rise to a certain degree of hysteresis [41]. Moreover, a fixture platform was carefully designed for sensitivity-based tensile testing. As shown in Fig. 3e, the sensor's capability to detect minimal strain variations was rigorously assessed by subjecting it to cyclic strains ranging from 0 % to 0.072 %, while simultaneously recording the ensuing alterations in resistance. The sensor reliably detected strain changes as small as 0.072 %, which is equivalent to a displacement of only 0.01 mm. These observations conclusively affirm the sensor's exceptional sensitivity, rendering it proficient in the precise detection of minuscule strains applicable in real-world scenarios. In order to assess the durability and longevity of the strain sensors, transient responses of relative resistance changes ($\Delta R/R_0$) were monitored during a series of repeated stretch-and-release cycles involving a 2 % tensile strain. Here, R_0 represents the initial resistance prior to strain application. It is pertinent to note that when the initial strain is applied, the silver film within the sensor experiences crack formation, which subsequently leads to an increase in resistance. Consequently, the initial resistance (R_0) exhibits an initial drift and subsequently reverts to a value lower than its original magnitude. In order to mitigate this phenomenon, a higher tensile strain of 3 % was employed during the pre-stretching to eliminate the influence of irreversible damage and establish a more consistent strain baseline. As shown in Fig. 3f, there was no significant difference in relative resistance changes even after 140,000 cycles. The inset in the figure demonstrates that there was no discernible change in the resistance change before and after the extended stability testing, proving the sensor's resilience and longevity in demanding operational environments. The dynamic response time, denoting the interval required for resistance to transition from 10 % to 90 %, is a pivotal parameter governing the sensor's performance in responding to external strains. Swift response characteristics hold substantial advantages, particularly in applications of real-time human movement monitoring and human-computer interaction. Fig. 3g exhibits a response time of 67 ms and a recovery time of 131 ms. The relatively longer recovery time is attributed to the inherent hysteresis tendencies inherent in stretchable polymers during the stretching process. In conclusion, the thickness of the PDMS substrate and the deposition thickness of the sensitive layer are considered as pivotal factors determining the performance of the strain sensors. Through the deliberate adjustment of these parameters, strain sensors can be designed to exhibit a range of sensitivities, while simultaneously maintaining diverse degrees of stability and reliability. The sensors still have high sensitivity compared to other work (Fig. S9). The strain-isolated PDMS substrates have demonstrated commendable performance in terms of stability, reproducibility, and response time, thereby making them suitable for practical applications demanding accurate and real-time strain detection.

Capitalizing on the amalgamation of electrical conductivity, flexibility, stretchability, and sustained stability inherent in the zoned substrate, the sensors have been carefully designed to mimic the skin's functionality, exhibiting the capability to respond dynamically to variable stimuli and facilitate real-time monitoring of human motions. Fig. 4 displays the sensor integration into the knuckle region of a finger, illustrating its ability to respond to various stimuli. The resistance change signals originating from the second knuckle of the index finger with five distinct motion states are exhibited in Fig. 4a. The stability and repeatability of the sensor are determined through repetitive finger movements, consisting of five repetitions for each state, respectively, thereby yielding five peak resistance. It ensures that each distinct motion state of the second knuckle of the index finger is reliably and precisely represented through the electrical resistance signals. Fig. 4b provides a visual testament to the strain sensor's remarkable sensitivity in discerning subtle changes in joint movements, as it responds precisely to even minute angular variations, demonstrating its efficiency in capturing subtle changes in joint motion. Furthermore, Fig. 4c displays the integrated three distinct sensors on the same substrate, each affixed to different finger joints, respectively. This sensor array achieved simultaneous tracking of strain variations in multiple joints, each involved in distinct gestures. This was prepared through the utilization of an interval-distributed partitioned PDMS substrate, where three sensors are seamlessly incorporated into the three joints of the little finger, as shown in Fig. 4d. This integrated setup offers the capability to discern and discriminate various finger movements. In addition, five sensors integrated into a glove enable the comprehensive analysis of the entire hand's finger movements. When multiple fingers engage in simultaneous motion, the movement data for each individual finger can be effectively translated into distinct resistance signals. By amalgamating these resistance signals from the five sensors, a composite resistance signal representing a specific gesture can be ascertained, as exemplified in Fig. 4e. The variations in resistance signals corresponding to diverse gestures, such as those denoted as gestures 1, 5, 6, and clenching, can be accurately identified. Importantly, it is imperative to note that the data acquisition channels associated with the five fingers remain independent of each other, ensuring that they do not mutually interfere during different gestures. In summary, through the adept use of the zoned substrate and the integration of multiple sensors into a unified device, the functionality of human skin could be simulated well by the strain sensors. Consequently, it represents in the recognition and comprehensive analysis of real-time human movements.

To further investigate the potential of the strain isolation substrate in the reorganization of external stimuli, we designed a 4 × 4 strain sensor array based on the strain isolation substrate. The preparation of the array is illustrated in Fig. S10, Supporting Information. This array serves as a versatile tool for perceiving the distribution of external stimuli, enabling the detection and localization of various stimuli patterns. Different mold shapes were employed to subject the sensing array to different stimuli patterns. When a cube was positioned at a specific pixel within the device, the relative resistance changes obtained by the 4 × 4 strain sensor array reflect the precise location of the applied stimulus, as displayed in Fig. 5a. This unique capability of the sensor array could detect and localize external stimuli. Moreover, Fig. 5b and Fig. S11 comprehensively exhibit the resistance responses, reflecting the

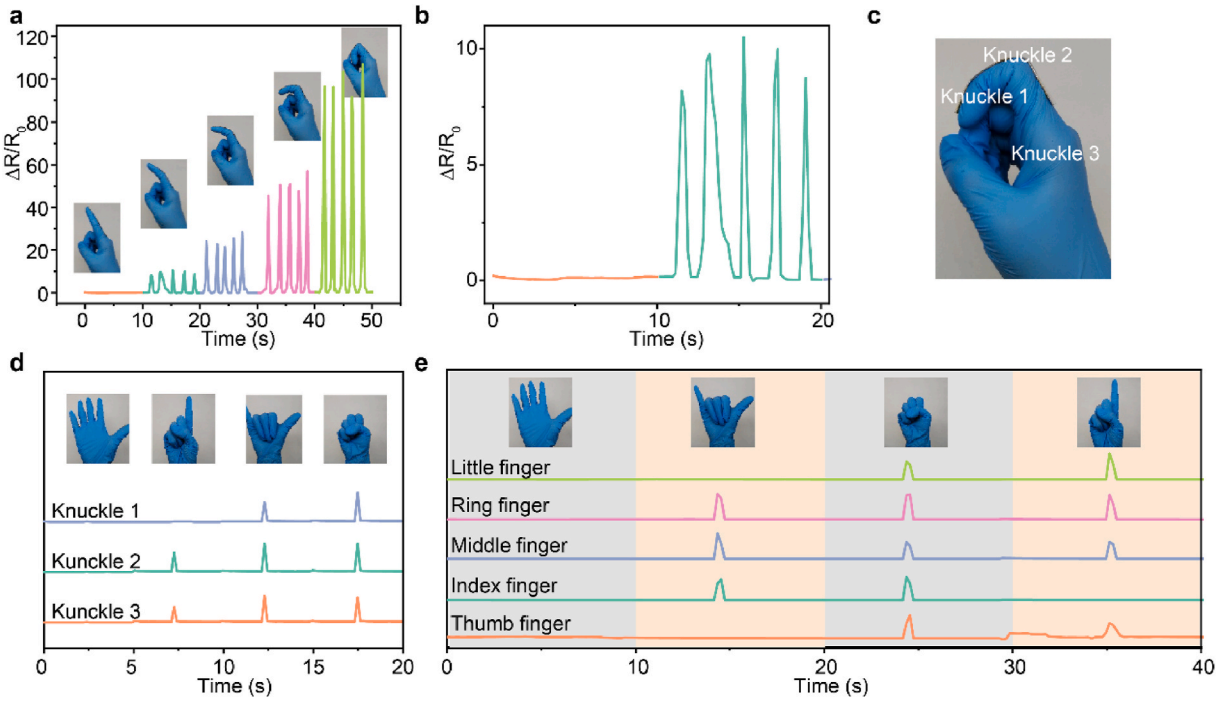

Fig. 4. Monitoring during finger motion. a) The response of a single strain sensor based on a strain-isolated substrate to progressive bending of the index finger (inset is a photograph of the finger with a strain-isolated sensor in a glove). b) The small-angle enlarged figure of a. c) Schematic diagram of the three knuckles of the finger. d) Motion detection of the three knuckles of the little finger. e) Finger motion detection.

characters "Z," "L," "C," and other shapes when applied as stimuli. It is noteworthy that, due to the effects of the stimulus point, adjacent pixels in the vicinity may also record resistance fluctuations, potentially influencing the precision of external stimulus identification. In summary, the strain isolation substrate, in combination with a sensor array demonstrates its immense potential in the realm of detecting and accurately localizing external stimuli. By further integrating these sensors into a glove and implementing machine learning algorithms, this technology stands poised to advance gesture recognition and facilitate precise grasping operation recognition.

The utilization of serpentine electrodes in device design brings forth a remarkable flexibility characteristic, endowing the electrodes with an extraordinary capacity for bending and stretching. This characteristic empowers electronic devices the ability to seamlessly conform to various geometric configurations, including curved surfaces, thereby substantially broadening their potential applications. Furthermore, serpentine electrodes offer a practical solution to the issue of conventional metal electrodes invariable even under minimal strain, thereby making them an optimal choice for integration into stretchable systems. In addition, their planar configuration aligns comfortably with Printed Circuit Board (PCB) bonding procedures, making them a widely adopted electrode structure in the field of stretchable electronics. Previous research endeavors encountered formidable challenges when integrating conventional rigid components into stretchable electronics that employ electrodes and flexible substrates. These challenges emanate from the inherent brittleness of rigid components and their mechanical and chemical incompatibilities with flexible substrates, frequently culminating in issues such as structural fracture and separation. In order to systematically address and overcome these formidable challenges, we have proposed an approach that capitalizes on the incorporation of serpentine electrodes within a framework complemented by strain isolation substrates. The distinctive geometry of serpentine electrodes plays a pivotal role in the alleviation of mechanical stress concentration and the mitigation of strain experienced by electronic devices during bending or stretching. This innovative design consequently enhances the overall stability and elasticity of the device. Meanwhile, the utilization of strain isolation substrates is considered as an effective strategy to enhance the overall stability of rigid components subjected to strain. In order to address these challenges, we have introduced two novel structural solutions, designated as Structure I and Structure II. Wherein, Structure I is characterized by a serpentine electrode composed of high Young's modulus PDMS enclosed within a low Young's modulus PDMS substrate, while Structure II involves a serpentine electrode made of low Young's modulus PDMS, enveloped by a high Young's modulus PDMS substrate. Both of these structural configurations exhibit notable enhancements in terms of strain isolation when compared to Structures III and IV, which are a high Young's modulus PDMS substrate and a low Young's modulus PDMS substrate, respectively, and do not possess inherent strain isolation capabilities. The discernible resistance changes under strain for these structures are represented in Fig. 5c, where Structures I and II demonstrate the significant decrease of resistance. To enhance understanding of the strain isolation capabilities inherent to Structure I and Structure II, we conducted finite element analysis. Fig. 5d exhibits the simulation results of four structures, respectively, which verified that there is a degree of strain isolation in both Structure I and II in comparison to the PDMS substrates without the partitioned structure. Through the comprehensive analysis, Structure I (a high Young's modulus PDMS electrode enclosed within a low Young's modulus PDMS) was considered as the preferred design meeting the specified requirements.

This method can be extended to the design of stretchable circuits by incorporating diverse patterns of high Young's modulus PDMS within low Young's modulus PDMS substrates. High Young's modulus regions of PDMS substrates serve as hosts for non-stretchable rigid components in conjunction with serpentine electrodes (Fig. 5e), thus safeguarding these rigid elements against strain-induced stresses. To demonstrate the practicality of this approach, a circuit was designed based on Structure I. The circuit, together with an LED, was strategically positioned on a rigid island to mitigate strain exerted on the LED during stretching, ensuring its stable operation. A comparative analysis was conducted between the circuit benefiting from strain isolation treatment (Structure I) and an identical circuit devoid of such treatment (Structure IV in Fig. 5c). As

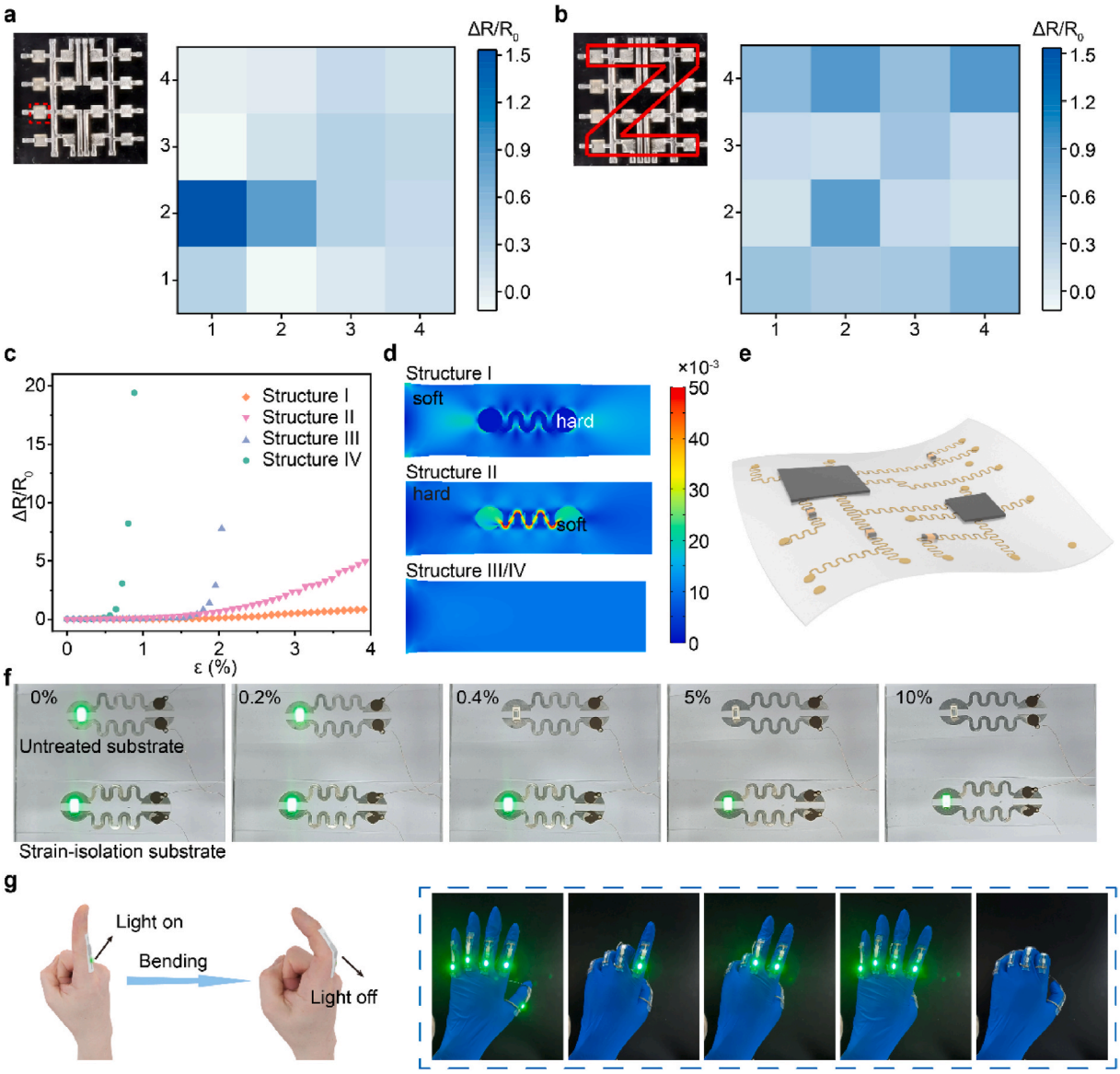

Fig. 5. Stretchable electronics based on strain isolation substrates. a) Detection of single point strain applied in a 4 × 4 array. b) Detection of multi-point strain applied in a 4 × 4 array. c) Relative resistance change as a function of tensile strain for different strain isolation structures. d) Finite element analysis of different strain isolated structures at 2 % strain. e) Schematic diagram of the stretchable circuit. f) Demonstration of a simple stretchable circuit. g) The direct control of the visualized signals of LEDs by finger bending.

shown in Fig. 5f, the circuit equipped with strain isolation treatment exhibited the remarkable capability of sustaining LED illumination even under a 10 % strain condition, with almost no change in brightness. In contrast, the circuit without strain isolation treatment exhibited electrical failure at a mere 0.4 % strain, leading to the abrupt extinguishing of the LED. This phenomenon serves as a compelling testament to the manifold advantages of the strain isolation strategy, which offers a feasible resolution for the integration of diverse systems. It clarified the substantial potential in the strain isolation methodology for flexible circuit integration, to enhance mechanical robustness and functional integrity.

To demonstrate the exceptional performance of our prepared strain-isolating substrates, we fabricated tactile gloves capable of visualizing finger movement (Fig. 5f). On each joint of these gloves, a micro-crack tactile sensor is positioned, accompanied by an LED mounted on a rigid island connected to it. The input strain is induced through finger bending, with each LED responsive to the corresponding finger's movement. This innovation is poised for integration into hand communication systems, as it empowers users to control LEDs directly through distinct finger actions. We successfully demonstrated that the unique movements of all five fingers can be employed to operate these LEDs. The glove holds great promise for the expansion of communication systems, facilitating interactions between humans, machines, and even machine-to-machine interfaces through straightforward hand gestures. Moreover, this system exhibits considerable potential for various biophotonic applications [42,43].

3. Conclusion

In this research, we have introduced an innovative strain-isolation strategy and developed strain-isolation substrates with various Young's moduli, with a notable maximum modulus ratio of 30 times within a single elastic substrate. This pioneering approach to integrating strain isolation effectively alleviates the occurrence of micro-cracks. In comparison to traditional flexible substrates, the substrates with strain isolation remarkably amplify the stability of interconnections between

rigid components and electrodes. Furthermore, they exhibit heightened tensile failure strain thresholds (120 %) and longer operational life (over 140,000 cycles) under strain conditions. This significant progress in strain isolation technology substantively supports the elasticity and longevity of stretchable systems, thereby rendering them more dependable for practical utilization. In addition, to cater to the diverse requirements of different applications, we have designed sensors with various sensitivity levels, allowing them to address the specific demands of different usage conditions. For the practical embodiment of a stretchable micro-crack strain sensing system, a stretchable sensing array was prepared to accurately distinguish a series of arrayed strain stimuli. This array achieved the capacity for precise detection and differentiation among various types of strains. Furthermore, we have designed serpentine electrodes featuring stretchability, serving as ideal platforms for the integration of rigid components such as LEDs onto rigid islands. This combination of rigid and stretchable elements exemplifies the versatility and potential of our technological advancement. As a consequence, our technology holds extensive applicability across a variety of stretchable electronic products, ensuring robust endurance in the diverse modes of deformation. This progress drives closer to the commercialization of stretchable electronic products, poised to cater to numerous practical functions while enhancing the adaptability of electronic devices.

4. Experiment section

4.1. Fabrication of the strain-isolating substrate

The fabrication process commenced by initially treating a glass substrate through immersion in a mixed solution of n-hexane and Octadecyl trichlorosilane (OTS) at a volume ratio of 200:1 for a duration of 25 min, followed by a meticulous cleansing procedure involving acetone and deionized water. Subsequently, a PDMS (Sylard 184, Dow Corning) mixture was meticulously prepared, adhering to the base/cross-linkers mass ratio of 20:1. The PDMS film was then meticulously created via the spin coating method, where it was applied to the previously treated glass substrate. The as-prepared PDMS film was placed into an oven environment set at 80 °C for 4 h, thereby forming a stretchable PDMS film. The thickness of the PDMS film falls within the range of 500–1000 μm, contingent upon the quality of the material before undergoing the curing process. To achieve the selective secondary curing of PDMS, the already cured PDMS film was covered the patterned Kapton mask prepared by a laser cutting. Next, the curing agent was uniformly spin-coated onto the PDMS film, with rotation speeds ranging from 500 to 5000 rpm/s for 60 s. Following this step, the composite material was subjected to a controlled temperature of 80 °C for 1 h. Finally, the Kapton mask was diligently removed, thereby yielding the selectively cured PDMS film. Finally, after a constant temperature of 80 °C for 1 h and carefully peeling off the Kapton mask, the selective curing PDMS film was prepared. Fabrication of Ag film on PDMS.

4.2. Fabrication of Ag film on PDMS

Firstly, an Ag film was meticulously deposited atop the PDMS film via magnetron sputtering, facilitated by the presence of a Kapton mask, for approximately 5 min, while operating at a sputtering power of 60 W. Secondly, the Kapton mask was removed, allowing for the subsequent step of Ag film deposition. Subsequently, an additional layer of Ag film was deposited with another specific patterned Kapton mask as, still operating at 60W of sputtering power, but with 3 min, via magnetron sputtering. Finally, after removing the Kapton mask, the as-prepared PDMS film was stripped easily which benefitted from surface treatment before and a strain sensor with parallel cracks was obtained by applying 10 % strain to pre-stretching.

4.3. Fabrication based on a strain-isolation substrate sensor array

Firstly, the glass substrate and a PDMS film were prepared according to the previously outlined method. Subsequently, a 500 μm-thick PDMS film was cured onto the suitably prepared glass surface. Next, Ag films, featuring various thicknesses, were deposited onto the PDMS film to serve as both the electrode and the sensitive layer, employing the same deposition technique detailed previously. Finally, an array comprising multiple micro-crack sensors was achieved through the application of pre-stretching.

CRediT authorship contribution statement

Xiaojun Pan: Writing – original draft, Validation, Conceptualization. **Jing Li:** Data curation. **Zhangsheng Xu:** Writing – review & editing. **Yue Liu:** Visualization. **Wenchao Gao:** Supervision, Conceptualization. **Rongrong Bao:** Supervision, Methodology, Conceptualization. **Caofeng Pan:** Writing – review & editing, Resources, Project administration, Funding acquisition.

Declaration of competing interest

The authors declare that they have no known competing financial interests or personal relationships that could have appeared to influence the work reported in this paper.

Data availability

Data will be made available on request.

Acknowledgements

The authors thank the support of Natural Science Foundation of Beijing (L223006 and 2222088), National Natural Science Foundation of China (No. 52203307, 52125205, U20A20166, 61805015, 61804011, 52202181 and 52102184), the National Key R&D Program of China (2021YFB3200302 and 2021YFB3200304), the Shenzhen Science and Technology Program (KQTD20170810105439418) and the Fundamental Research Funds for the Central Universities for their support.

Appendix A. Supplementary data

Supplementary data to this article can be found online at https://doi.org/10.1016/j.mtphys.2024.101562.

References

[1] R. Bao, J. Tao, J. Zhao, M. Dong, J. Li, C. Pan, Integrated intelligent tactile system for a humanoid robot, Sci. Bull. 68 (2023) 1027–1037, https://doi.org/10.1016/j.scib.2023.04.019.

[2] K. Chen, K. Liang, H. Liu, R. Liu, Y. Liu, S. Zeng, Y. Tian, Skin-Inspired ultra-tough supramolecular multifunctional hydrogel electronic skin for human–machine interaction, Nano-Micro Lett. 15 (2023) 102, https://doi.org/10.1007/s40820-023-01084-8.

[3] D. Hu, F. Giorgio-Serchi, S. Zhang, Y. Yang, Stretchable e-skin and transformer enable high-resolution morphological reconstruction for soft robots, Nat. Mach. Intell. 5 (2023) 261–272, https://doi.org/10.1038/s42256-023-00622-8.

[4] R. Bao, J. Tao, C. Pan, Z.L. Wang, Piezophototronic effect in nanosensors, Small Sci 1 (2021): 2000060, https://doi.org/10.1002/smsc.202000060.

[5] J. He, R. Wei, X. Ma, W. Wu, X. Pan, J. Sun, J. Tang, Z. Xu, C. Wang, C. Pan, Contactless user-interactive sensing display for human–human and human–machine interactions, Adv. Mater. 36 (2024): 2401931, https://doi.org/10.1002/adma.202401931.

[6] Y. Lu, X. Qu, W. Zhao, Y. Ren, W. Si, W. Wang, Q. Wang, W. Huang, X. Dong, Highly stretchable, elastic, and sensitive MXene-based hydrogel for flexible strain and pressure sensors, Research 2020 (2020): 2038560, https://doi.org/10.34133/2020/2038560.

[7] G. Ge, Y. Lu, X. Qu, W. Zhao, Y. Ren, W. Wang, Q. Wang, W. Huang, X. Dong, Muscle-Inspired self-healing hydrogels for strain and temperature sensor, ACS Nano 14 (2020) 218–228, https://doi.org/10.1021/acsnano.9b07874.

[8] J. Ren, W. Zhang, Y. Wang, Y. Wang, J. Zhou, L. Dai, M. Xu, A graphene rheostat for highly durable and stretchable strain sensor, InfoMat 1 (2019) 396–406, https://doi.org/10.1002/inf2.12030.
[9] R. Cao, Y. Liu, H. Li, Z. Shen, F. Li, X. Jia, C. Chen, R. Liu, C. Luo, W. Yang, R. Bao, C. Pan, Advances in high-temperature operatable triboelectric nanogenerator, SusMat 4 (2024) e196, https://doi.org/10.1002/sus2.196.
[10] R. Han, Y. Liu, Y. Mo, H. Xu, Z. Yang, R. Bao, C. Pan, High anti-jamming flexible capacitive pressure sensors based on core–shell structured AgNWs@TiO2, Adv. Funct. Mater. 33 (2023): 2305531, https://doi.org/10.1002/adfm.202305531.
[11] G. Ge, W. Yuan, W. Zhao, Y. Lu, Y. Zhang, W. Wang, P. Chen, W. Huang, W. Si, X. Dong, Highly stretchable and autonomously healable epidermal sensor based on multi-functional hydrogel frameworks, J. Mater. Chem. A 7 (2019) 5949–5956, https://doi.org/10.1039/C9TA00641A.
[12] Y. Liu, J. Tao, Y. Mo, R. Bao, C. Pan, Ultrasensitive touch sensor for simultaneous tactile and slip sensing, Adv. Mater. 36 (2024): 2313857, https://doi.org/10.1002/adma.202313857.
[13] G. Wu, X. Li, R. Bao, C. Pan, Innovations in tactile sensing: microstructural designs for superior flexible sensor performance, Adv. Funct. Mater. n/a (2024): 2405722, https://doi.org/10.1002/adfm.202405722.
[14] Y. Liu, R. Bao, J. Tao, J. Li, M. Dong, C. Pan, Recent progress in tactile sensors and their applications in intelligent systems, Sci. Bull. 65 (2020) 70–88, https://doi.org/10.1016/j.scib.2019.10.021.
[15] Y. Deng, X. Guo, Y. Lin, Z. Huang, Y. Li, Dual-phase inspired soft electronic sensors with programmable and tunable mechanical properties, ACS Nano 17 (2023) 6423–6434, https://doi.org/10.1021/acsnano.2c11245.
[16] H. Sun, Y. Bu, H. Liu, J. Wang, W. Yang, Q. Li, Z. Guo, C. Liu, C. Shen, Superhydrophobic conductive rubber band with synergistic dual conductive layer for wide-range sensitive strain sensor, Sci. Bull. 67 (2022) 1669–1678, https://doi.org/10.1016/j.scib.2022.07.020.
[17] Z. Xu, X. Pan, H. Lu, Q. Lu, Y. Liang, Z. He, Y. Zhu, Y. Yu, W. Wu, X. Han, C. Pan, Surface energy-assisted patterning of vapor deposited all-inorganic perovskite arrays for wearable optoelectronics, Adv. Sci. 11 (2024): 2402635, https://doi.org/10.1002/advs.202402635.
[18] K. Zhai, H. Wang, Q. Ding, Z. Wu, M. Ding, K. Tao, B.-R. Yang, X. Xie, C. Li, J. Wu, High-performance strain sensors based on organohydrogel microsphere film for wearable human–computer interfacing, Adv. Sci. 10 (2023): 2205632, https://doi.org/10.1002/advs.202205632.
[19] L. Liu, S. Niu, J. Zhang, Z. Mu, J. Li, B. Li, X. Meng, C. Zhang, Y. Wang, T. Hou, Z. Han, S. Yang, L. Ren, Bioinspired, omnidirectional, and hypersensitive flexible strain sensors, Adv. Mater. 34 (2022): 2200823, https://doi.org/10.1002/adma.202200823.
[20] K. Han, D. Zhang, W. Zhuang, Y. Wan, P. Yang, Integrated multimodal microfluidic E-skin powered by synergistic tandem nanogenerators for sweat health monitor and skin temperature analysis, J. Mater. Chem. A 11 (2023) 17112–17124, https://doi.org/10.1039/D3TA01755A.
[21] T. Zhang, Y. Ding, C. Hu, M. Zhang, W. Zhu, C.R. Bowen, Y. Han, Y. Yang, Self-Powered stretchable sensor arrays exhibiting magnetoelasticity for real-time human–machine interaction, Adv. Mater. n/a (2022): 2203786, https://doi.org/10.1002/adma.202203786.
[22] X. Huang, W. Guo, S. Liu, Y. Li, Y. Qiu, H. Fang, G. Yang, K. Zhu, Z. Yin, Z. Li, H. Wu, Flexible mechanical metamaterials enabled electronic skin for real-time detection of unstable grasping in robotic manipulation, Adv. Funct. Mater. 32 (2022): 2109109, https://doi.org/10.1002/adfm.202109109.
[23] C. Wang, R. Ma, D. Peng, X. Liu, J. Li, B. Jin, A. Shan, Y. Fu, L. Dong, W. Gao, Z. L. Wang, C. Pan, Mechanoluminescent hybrids from a natural resource for energy-related applications, InfoMat 3 (2021) 1272–1284, https://doi.org/10.1002/inf2.12250.
[24] R. Wei, J. He, S. Ge, H. Liu, X. Ma, J. Tao, X. Cui, X. Mo, Z. Li, C. Wang, C. Pan, Self-Powered all-optical tactile sensing platform for user-interactive interface, Adv. Mater. Technol. 8 (2023): 2200757, https://doi.org/10.1002/admt.202200757.
[25] M. Kim, J.J. Park, C. Cho, S.H. Ko, Liquid metal based stretchable room temperature soldering sticker patch for stretchable electronics integration, Adv. Funct. Mater. n/a (2023): 2303286, https://doi.org/10.1002/adfm.202303286.
[26] Y. Jiang, S. Ji, J. Sun, J. Huang, Y. Li, G. Zou, T. Salim, C. Wang, W. Li, H. Jin, J. Xu, S. Wang, T. Lei, X. Yan, W.Y.X. Peh, S.-C. Yen, Z. Liu, M. Yu, H. Zhao, Z. Lu, G. Li, H. Gao, Z. Liu, Z. Bao, X. Chen, A universal interface for plug-and-play assembly of stretchable devices, Nature 614 (2023) 456–462, https://doi.org/10.1038/s41586-022-05579-z.
[27] N. Naserifar, P.R. LeDuc, G.K. Fedder, Material gradients in stretchable substrates toward integrated electronic functionality, Adv. Mater. 28 (2016) 3584–3591, https://doi.org/10.1002/adma.201505818.
[28] C. Shang, Q. Xu, N. Liang, J. Zhang, L. Li, Z. Peng, Multi-parameter e-skin based on biomimetic mechanoreceptors and stress field sensing, npj Flexible Electron. 7 (2023) 19, https://doi.org/10.1038/s41528-023-00252-5.
[29] S. Wang, J. Xu, W. Wang, G.-J.N. Wang, R. Rastak, F. Molina-Lopez, J.W. Chung, S. Niu, V.R. Feig, J. Lopez, T. Lei, S.-K. Kwon, Y. Kim, A.M. Foudeh, A. Ehrlich, A. Gasperini, Y. Yun, B. Murmann, J.B.H. Tok, Z. Bao, Skin electronics from scalable fabrication of an intrinsically stretchable transistor array, Nature 555 (2018) 83–88, https://doi.org/10.1038/nature25494.
[30] L. Yin, S.S. Sandhu, R. Liu, M.I. Khan, C. Wicker, V. Garcia-Gradilla, J. Zhou, A.-Y. Chang, S. Wu, J.-M. Moon, C. Chen, S. Ding, J. Wang, Wearable E-skin microgrid with battery-based, self-regulated bioenergy module for epidermal sweat sensing, Adv. Energy Mater. 13 (2023): 2203418, https://doi.org/10.1002/aenm.202203418.
[31] T. Kim, H. Lee, W. Jo, T.-S. Kim, S. Yoo, Realizing stretchable OLEDs: a hybrid platform based on rigid island arrays on a stress-relieving bilayer structure, Adv. Mater. Technol. 5 (2020): 2000494, https://doi.org/10.1002/admt.202000494.
[32] Y. Kim, J. Kim, C.Y. Kim, T. Kim, C. Lee, K. Jeong, W. Jo, S. Yoo, T.-S. Kim, K. C. Choi, S.G. Im, A modulus-engineered multi-layer polymer film with mechanical robustness for the application to highly deformable substrate platform in stretchable electronics, Chem. Eng. J. 431 (2022): 134074, https://doi.org/10.1016/j.cej.2021.134074.
[33] N. Rodeheaver, R. Herbert, Y.-S. Kim, M. Mahmood, H. Kim, J.-W. Jeong, W.-H. Yeo, Strain-isolating materials and interfacial physics for soft wearable bioelectronics and wireless, motion artifact-controlled health monitoring, Adv. Funct. Mater. 31 (2021): 2104070, https://doi.org/10.1002/adfm.202104070.
[34] H. Hwang, M. Kong, K. Kim, D. Park, S. Lee, S. Park, H.-J. Song, U. Jeong, Stretchable anisotropic conductive film (S-ACF) for electrical interfacing in high-resolution stretchable circuits, Sci. Adv. 7 (2021): eabh0171, https://doi.org/10.1126/sciadv.abh0171.
[35] J.C. Yang, S. Lee, B.S. Ma, J. Kim, M. Song, S.Y. Kim, D.W. Kim, T.-S. Kim, S. Park, Geometrically engineered rigid island array for stretchable electronics capable of withstanding various deformation modes, Sci. Adv. 8 (2022), https://doi.org/10.1126/sciadv.abn3863 eabn3863.
[36] W. Wang, Y. Jiang, D. Zhong, Z. Zhang, S. Choudhury, J.-C. Lai, H. Gong, S. Niu, X. Yan, Y. Zheng, C.-C. Shih, R. Ning, Q. Lin, D. Li, Y.-H. Kim, J. Kim, Y.-X. Wang, C. Zhao, C. Xu, X. Ji, Y. Nishio, H. Lyu, J.B.H. Tok, Z. Bao, Neuromorphic sensorimotor loop embodied by monolithically integrated, low-voltage, soft e-skin, Science 380 (2023) 735–742, https://doi.org/10.1126/science.ade0086.
[37] D. Kang, P.V. Pikhitsa, Y.W. Choi, C. Lee, S.S. Shin, L. Piao, B. Park, K.-Y. Suh, T.-i. Kim, M. Choi, Ultrasensitive mechanical crack-based sensor inspired by the spider sensory system, Nature 516 (2014) 222–226, https://doi.org/10.1038/nature14002.
[38] T. Sekitani, U. Zschieschang, H. Klauk, T. Someya, Flexible organic transistors and circuits with extreme bending stability, Nat. Mater. 9 (2010) 1015–1022, https://doi.org/10.1038/nmat2896.
[39] J. Li, R.R. Bao, J. Tao, M. Dong, Y.F. Zhang, S. Fu, D.F. Peng, C.F. Pan, Visually aided tactile enhancement system based on ultrathin highly sensitive crack-based strain sensors, Appl. Phys. Rev. 7 (2020): 011404, https://doi.org/10.1063/1.5129468.
[40] B. Park, J. Kim, D. Kang, C. Jeong, K.S. Kim, J.U. Kim, P.J. Yoo, T.-i. Kim, Dramatically enhanced mechanosensitivity and signal-to-noise ratio of nanoscale crack-based sensors: effect of crack depth, Adv. Mater. 28 (2016) 8130–8137, https://doi.org/10.1002/adma.201602425.
[41] Y.-L. Rao, A. Chortos, R. Pfattner, F. Lissel, Y.-C. Chiu, V. Feig, J. Xu, T. Kurosawa, X. Gu, C. Wang, M. He, J.W. Chung, Z. Bao, Stretchable self-healing polymeric dielectrics cross-linked through metal–ligand coordination, J. Am. Chem. Soc. 138 (2016) 6020–6027, https://doi.org/10.1021/jacs.6b02428.
[42] G.-H. Lee, C. Jeon, J.W. Mok, S. Shin, S.-K. Kim, H.H. Han, S.-J. Kim, S.H. Hong, H. Kim, C.-K. Joo, J.-Y. Sim, S.K. Hahn, Smart wireless near-infrared light emitting contact lens for the treatment of diabetic retinopathy, Adv. Sci. 9 (2022): 2103254, https://doi.org/10.1002/advs.202103254.
[43] G.-H. Lee, H. Moon, H. Kim, G.H. Lee, W. Kwon, S. Yoo, D. Myung, S.H. Yun, Z. Bao, S.K. Hahn, Multifunctional materials for implantable and wearable photonic healthcare devices, Nat. Rev. Mater. 5 (2020) 149–165, https://doi.org/10.1038/s41578-019-0167-3.